Inorganic Chemistry

Article

pubs.acs.org/IC

Crystal Structure and Highly Luminescent Properties Studies of Bis-β-diketonate Lanthanide Complexes

Jing Shi, Yanjun Hou,* Wenyi Chu, Xiaohong Shi, Huiquan Gu, Bilin Wang, and Zhizhong Sun*

Key Laboratory of Chemical Engineering Process and Technology for High-Efficiency Conversion, School of Chemistry and Materials Science, Heilongjiang University, No.74, Xuefu Road, Nangang District, Harbin 150080, People's Republic of China

Supporting Information

ABSTRACT: A new bis(β-diketonate), 1,3-bis(4,4,4-trifluoro-1,3-dioxobutyl)phenyl (BTP), which contains a trifluorinated alkyl group, has been prepared for the synthesis of two series of dinuclear lanthanide complexes with the general formula $Ln_2(BTP)_3L_2$ [Ln^{3+} = Eu^{3+}, L = DME(**1**), bpy(**2**), and phen(**3**); Ln^{3+} = Sm^{3+}, L = DME(**4**), bpy(**5**), and phen(**6**); DME = ethylene glycol dimethyl ether, bpy = 2,2′-bipyridine, phen = 1,10-phenanthroline]. The crystal structure of the free ligand has been determined and shows a twisted arrangement of the two binding sites around the 1,3-phenylene spacer. X-ray crystallographic analysis reveals that complexes **1**, **2**, **4**, and **5** are triple-stranded dinuclear structures formed by three bis-bidentate ligands with two lanthanide ions. The room-temperature photoluminescence (PL) spectra of complexes **1**−**6** show that this bis-β-diketonate can effectively sensitize rare earths (Sm^{3+} and Eu^{3+}) and produce characteristic emissions of the corresponding Eu^{3+} and Sm^{3+} ions. In addition, two bidentate nitrogen ancillary ligands, 2,2′-bipyridine (bpy) and 1,10-phenanthroline (phen), have been employed to enhance the luminescence quantum yields and lifetimes of both series of Eu^{3+} and Sm^{3+} complexes.

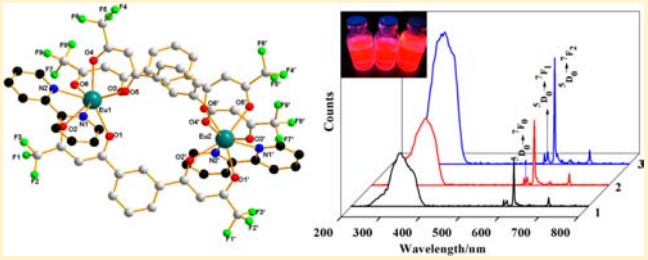

INTRODUCTION

Extensive interest has been focused on the investigation of photophysical properties of lanthanide ions owing to the widespread applications in display devices, luminescent sensors, probes for clinical use, tunable lasers, optical amplifiers, and efficient light conversion molecular devices, to name a few.[1−6] The current increasing interest in lanthanide β-diketonate complexes has been received due to high molar absorption coefficients of the β-diketonate ligands, long luminescent lifetimes, and high luminescence quantum efficiency.[7,8] On one hand, bis-β-diketonate ligands have more negatively charged binding sites, which can form stable triple-stranded dinuclear structures. On the other hand, bis-β-diketonate ligands can effectively transfer the intramolecular energy to the central ion, contributing to bringing characteristic luminescence properties.[9] Previously, various β-diketonate ligands have been documented,[10] and thenoyltrifluoroacetone (TTA) and acylpyrazole derivates are the most famous β-diketonate ligands for sensitizing Eu^{3+} luminescence.[11] But there exist few studies of bis-β-diketonate lanthanide complexes with triple-stranded dinuclear helicate structure.[12] Bassett et al. have prepared two bis-β-diketonate ligands for examination of dinuclear lanthanide complex formation and investigation of their properties as sensitizers for lanthanide luminescence.[13] However, it is a pity that no crystallographic data are available for the proposed triple-stranded dinuclear structure; only molecular simulation structure is shown. Recently, Li et al. have shown that a europium bis-β-diketonate complex exhibited a 1.33 times more intense luminescence signal than the corresponding mononuclear analogue.[14] But we found that only triple-stranded dinuclear lanthanide complexes are proved by single crystal X-ray diffraction. In contrast, we report not only four single crystal structures of triple-stranded dinuclear lanthanide complexes but also that the luminescence signal of the europium BTP complex is 1.67 times more than that of corresponding mononuclear analogue. Additionally, we display that the quantum yields of complexes **2** and **3** are higher than that of the corresponding analogue, which are illustrated in Table 3.

We all know that the energy of C−H oscillators required is more than that of C−F oscillators, resulting in lower luminescence intensities and shorter excited-state lifetimes. Thus, the replacement of the C−H bonds with lower-energy C−F oscillators plays a critical role in the design of high performance luminescent molecular devices.[15,16] Additionally, the β-diketonate ligand is one of the important "antennas" which effectively transfer the energy of the ligand to metal; the lanthanide-centered luminescent properties are enhanced.

On the basis of the above-mentioned consideration, we sought a new bis-β-diketonate, 1,3-bis(4,4,4-trifluoro-1,3-dioxobutyl)phenyl (BTP), ligand for the formation of dinuclear lanthanide complexes, which is composed of the highly electron-withdrawing $-CF_3$ groups, which minimize the energy

Received: December 12, 2012
Published: April 19, 2013

dx.doi.org/10.1021/ic302726z | Inorg. Chem. 2013, 52, 5013−5022

Table 1. Crystal Data and Structure Refinement for Complexes 1, 2, 4, and 5

parameters	1	2	4	5
formula	$C_{50}H_{38}Eu_2F_{18}O_{16}$	$C_{64}H_{38}Eu_2F_{18}N_4O_{12}Cl_4$	$C_{50}H_{38}Sm_2F_{18}O_{16}$	$C_{62}H_{34}Sm_2F_{18}N_4O_{12}Cl_4$
M_r	1540.72	1842.70	1537.50	1839.48
color	buff	buff	buff	buff
cryst syst	monoclinic	monoclinic	monoclinic	monoclinic
space group	$C2/c$	$P\bar{1}$	$C2/c$	$P\bar{1}$
a (Å)	15.632(3)	12.3302(4)	15.6073(8)	12.3311(4)
b (Å)	12.913(2)	15.1832(5)	12.9464(6)	15.1841(5)
c (Å)	29.373(5)	19.6047(7)	29.3024(14)	19.6059(7)
α (deg)	90	96.92	90	96.92
β (deg)	92.006(2)	103.56	92.0160(10)	103.56
γ (deg)	90	91.55	90	91.55
V (Å^3)	5925.6(18)	3536.0(2)	5917.1(5)	3536.7(2)
Z	4	2	4	2
ρ (g cm^3)	1.727	1.731	1.726	1.727
μ (mm^{-1})	2.217	2.017	2.085	1.904
F (000)	3016	1804	3008	1800
R_1 [$I > 2\sigma(I)$]	0.0425	0.0329	0.0297	0.0356
wR_2 [$I > 2\sigma(I)$]	0.1125	0.0876	0.0656	0.0965
R_1 (all data)	0.0532	0.0381	0.0332	0.0408
wR_2 (alldat)	0.1204	0.0919	0.0672	0.1013
GOF on F^2	1.035	1.038	1.159	1.034

losses compared with C−H bonds, that could better promote the solubility of bis-β-diketonate lanthanide complexes in different organic solvents. Further investigation of photoluminescence studies reveals that bis-β-diketonate complex $[Eu_2(BTP)_3(H_2O)_4]$ exhibited a 1.67 times more intense luminescence signal than the corresponding mononuclear analogue $[Eu(BTFA)_3(H_2O)_2]$.

EXPERIMENTAL SECTION

Materials and Instrumentation. The commercially available chemicals were analytical reagent grade and used without further purification. $LnCl_3{\cdot}6H_2O$ was prepared according to the literature by dissolving lanthanide oxide in a slight excess of hydrochloric acid. The solution was evaporated, and the precipitate was collected from water.[13] Elemental analyses were performed on an Elementar Vario EL cube analyzer. Fourier transform infrared (FT-IR) spectra were obtained on a Perkin-Elmer Spectrum One spectrophotometer by using KBr disks in the range 4000−370 cm^{-1}. Ultraviolet (UV) spectra were recorded on a Perkin-Elmer Lambda 25 spectrometer. Thermal analyses were conducted on a Perkin-Elmer STA 6000 with a heating rate of 10 °C·min^{-1} in a temperature range from 30 to 800 °C under a N_2 atmosphere. The ^{1}H NMR spectra were recorded on a Bruker Avance III 400 MHz spectrometer in $CDCl_3$ solution. Excitation and emission spectra were measured by an Edinburgh FLS 920 fluorescence spectrophotometer. Luminescence lifetimes were recorded on a single photon counting spectrometer from Edinburgh Instrument (FLS 920) with a microsecond pulse lamp as the excitation. The data were analyzed by software supplied by Edinburgh Instruments. Suitable single crystals of **1**, **2**, **4**, and **5** were selected for single crystal diffraction analysis (CCDC Nos. 886032, 899276, 898750, and 899343 contain supplementary crystallographic data for complexes **1**, **2**, **4**, and **5**). Diffraction intensity data were collected on a Bruker SMART APEX II X-ray diffractometer with graphite-monochromated Mo Kα radiation (l = 0.71073 Å). All data were collected at a temperature of 20 ± 2 °C. The structures were solved using direct methods and refined on F^2 by full-matrix least-squares using the SHELXTL-97 program. The Ln^{3+} ions were easily located, and then non-hydrogen atoms (C, N, O, and F) were placed from the subsequent Fourier-difference maps. A summary for data collection and refinements is given in Table 1. The overall quantum yields of both europium and samarium complexes were measured in CH_3CN at room temperature and cited relative to a reference solution of $Ru(bpy)_3Cl_2$ (Φ = 55.3%),[17] and through the following expression:

$$\varphi_{overall} = \frac{n^2 A_{ref} I}{n_{ref}^2 A I_{ref}} \varphi_{ref} \quad (1)$$

In eq 1, n, I, and A denote the refractive index of solvent, the area of the emission spectrum, and the absorbance at the excitation wavelength, respectively, and φ_{ref} represents the quantum yield of the standard $Ru(bpy)_3Cl_2$ solution. The subscript ref denotes the reference, and the absence of a subscript implies an unknown sample.

Synthesis of 1,3-bis(4,4,4-trifluoro-1,3-dioxobutyl)phenyl (BTP). A mixture of sodium ethoxide (1.4 g, 20 mmol) and ethyl trifluoroacetate (2.9 g, 20 mmol) in 40 mL of dry THF (tetrahydrofuran) was stirred for 10 min, followed by the addition of 1,3-bis-acetophenone (2.97 g, 8.4 mmol). Then, it was further stirred at room temperature for 24 h (Scheme 1). The resulting mixture was poured into 100 mL of ice water and acidified to pH 2−3 using hydrochloric acid (2 M), and the resulting white precipitate was filtered and dried in a vacuum. Recrystallization from isopropanol gave white flake crystals (2.7 g, 82%). Elemental analysis (%) calcd for $C_{14}H_8F_6O_4$ (354.03): C, 47.47; H, 2.28. Found: C, 47.45; H, 2.29. IR (KBr, cm^{-1}): 3435 (w), 3125 (w), 1591 (s), 1269 (s), 1207 (s), 1158 (s), 1080 (s), 93 (m), 787 (m), 723 (w), 709 (w), 678 (w), 627 (m), 577 (m). 1HNMR ($CDCl_3$, 400 MHz): 14.83 (s, 2H), 8.49 (s, 1H), 8.16 (d, J = 1.0 Hz, 2H), 7.68 (t, J = 2.0 Hz, 1H), 6.64 ppm (s, 2H) (Figure S1, Supporting Information). ESI-TOF m/z = 354 (M^-) (Figure S2, Supporting Information).

Scheme 1. Synthesis of the BTP

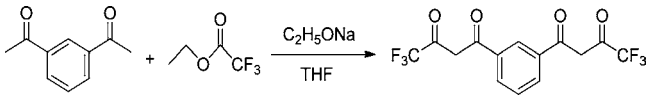

Synthesis of $Gd_2(BTP)_3(H_2O)_4$. An aqueous solution of $GdCl_3{\cdot}6H_2O$ (1.0 mmol) was added to a solution of BTP (1.5 mmol) in methanol in the presence of NaOH (1.5 mmol). Precipitation took place immediately, and the reaction mixture was stirred for 10 h at room temperature. The product was filtered; washed with methanol, water, and then methanol; dried; and stored in a desiccator. The complex was then purified by recrystallization from a

dx.doi.org/10.1021/ic302726z | Inorg. Chem. 2013, 52, 5013−5022

Scheme 2. Synthesis of Complexes 1−6

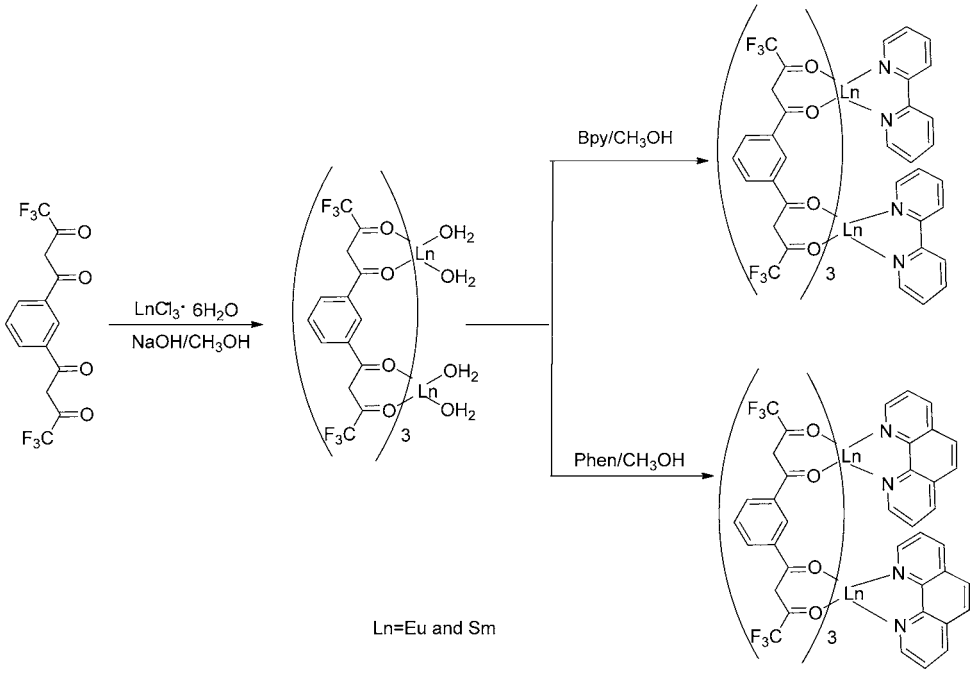

dichloromethane−methanol mixture. Yield: 82%. Elemental analysis (%) calcd for $C_{42}H_{32}Gd_2F_{18}O_{16}$ (1449.99): C, 34.81; H, 2.23. Found: C, 34.83; H, 2.24. IR (KBr)ν_{max}: 3419 cm^{-1} (s, ν_{O-H}), 1619 cm^{-1} (s, $\nu_{C=O}$), 1538 cm^{-1} (s), 1294 cm^{-1} (s), 1137 cm^{-1} (s, ν_{C-F}), 783 cm^{-1} (m, ν_{CF3}).

Synthesis of $Gd(bpy)_2(NO_3)_3$. To a 50 mL methanol solution containing 2,2′-bipyridine (2.0 mmol), $Gd(NO_3)_3(H_2O)_6$ (1.0 mmol) was added dropwise under constant stirring, and then, the solution was refluxed for 1 h at 65 °C. The resulting solution was filtered to obtain a white powder. Yield: 85%. Elemental analysis (%) calcd for $C_{20}H_{20}GdN_6O_6$ (597.70): C, 40.19; H, 3.37; N, 14.06. Found: C, 40.18; H, 3.38; N, 14.06. IR (KBr) ν_{max}: 1578 cm^{-1} (s, ν_{N-O}), 1458 cm^{-1} (s), 1415 cm^{-1} (s), 1312 cm^{-1} (s), 1039 cm^{-1} (s, ν_{C-N}), 757 cm^{-1} (m, ν_{N-O}).

Synthesis of $Gd(phen)_2(NO_3)_3$. To a 50 mL methanol solution containing 1,10-phenanthroline (2.0 mmol), $Gd(NO_3)_3(H_2O)_6$ (1.0 mmol) was added dropwise under constant stirring, and then, the solution was refluxed for 1 h at 65 °C. The resulting solution was filtered to obtain a white powder. Yield: 89%. Elemental analysis (%) calcd for $C_{24}H_{20}GdN_6O_6$ (645.70): C, 44.64; H, 3.12; N, 14.87. Found: C, 44.66; H, 3.11; N, 14.86. IR (KBr) ν_{max}: 1559 cm^{-1} (s, ν_{N-O}), 1422 cm^{-1} (s), 1295 cm^{-1} (s), 1026 cm^{-1} (s, ν_{C-N}), 739 cm^{-1} (m, ν_{N-O}).

Synthesis of $Eu_2(BTP)_3(H_2O)_4$ and $Sm_2(BTP)_3(H_2O)_4$. To a methanol solution of BTP (1g, 2.8 mmol), NaOH (0.2 g, 5.6 mmol) was added, and the mixture was allowed to stir for 5 min. To this methanol solution, $LnCl_3{\cdot}6H_2O$ (1.86 mmol) was added dropwise, and the mixture was allowed to stir for 24 h at ambient temperature. Water was then added to this mixture, and the precipitate thus formed was filtered, washed with water, and dried in the air. Single crystals were obtained in about two weeks by recrystallization from DME/hexane.

$Eu_2(BTP)_3(H_2O)_4$. Yield: 87%. Elemental analysis (%) calcd for $C_{42}H_{32}Eu_2F_{18}O_{16}$ (1438.59): C, 35.07; H, 2.24. Found: C, 35.08; H, 2.24. IR (KBr)ν_{max}: 3420 cm^{-1} (s, ν_{O-H}), 1619 cm^{-1} (s, $\nu_{C=O}$), 1539 cm^{-1} (s), 1294 cm^{-1} (s), 1136 cm^{-1} (s, ν_{C-F}), 783 cm^{-1} (m, ν_{CF3}).

$Sm_2(BTP)_3(H_2O)_4$. Yield: 87%. Elemental analysis (%) calcd for $C_{42}H_{32}Sm_2F_{18}O_{16}$ (1435.39): C, 35.14; H, 2.25. Found: C, 35.15; H, 2.24. IR (KBr)ν_{max}: 3419 cm^{-1} (s, ν_{O-H}), 1620 cm^{-1} (s, $\nu_{C=O}$), 1536 cm^{-1} (s), 1293 cm^{-1} (s), 1137 cm^{-1} (s, ν_{C-F}), 781 cm^{-1} (m, ν_{CF3}).

$Eu_2(BTP)_3(DME)_2$ (1). Elemental analysis (%) calcd for $C_{50}H_{38}Eu_2F_{18}O_{16}$ (1540.72): C, 38.98; H, 2.49. Found: C, 38.97; H, 2.51. IR (KBr) ν_{max}: 1619 cm^{-1} (s, $\nu_{C=O}$), 1537 cm^{-1} (s), 1293 cm^{-1}(s), 1137 cm^{-1} (s, ν_{C-F}), 782 cm^{-1} (m, ν_{CF3}).

$Sm_2(BTP)_3(DME)_2$ (4). Elemental analysis (%) calcd for $C_{50}H_{38}Sm_2F_{18}O_{16}$ (1537.50): C, 39.06; H, 2.49. Found: C, 39.04; H, 246. IR (KBr) ν_{max}: 1621 cm^{-1} (s, $\nu_{C=O}$), 1538 cm^{-1} (s), 1294 cm^{-1} (s), 1137 cm^{-1} (s, ν_{C-F}), 781 cm^{-1} (m, ν_{CF3}).

Synthesis of 2, 3, 5, and 6. Complexes **2**, **3**, **5**, and **6** were prepared by stirring solutions of $Ln_2(BTP)_3(H_2O)_4$ and the two molar nitrogen donors in CH_3OH for 10 h at 65 °C. The products were isolated and purified following the aforementioned method. Single crystals of complexes **2** and **5** were harvested in about two weeks by recrystallization from chloroform and acetone/hexane.

$Eu_2(BTP)_3(bpy)_2(CH_2Cl_2)_2$ (2). Yield: 91%. Elemental analysis (%) calcd for $C_{64}H_{38}Eu_2F_{18}N_4O_{12}Cl_4$ (1842.70): C, 41.71; H, 2.08; N, 3.04. Found: C, 41.73; H, 2.07; N, 3.06. IR (KBr) ν_{max}: 1618 cm^{-1} (s, $\nu_{C=O}$), 1327 cm^{-1} (s), 1281 cm^{-1} (s), 1128 cm^{-1} (s, ν_{C-F}), 755 cm^{-1} (m, ν_{CF3}).

$Eu_2(BTP)_3(phen)_2$ (3). Yield: 89%. Elemental analysis (%) calcd for $C_{66}H_{34}Eu_2F_{18}N_4O_{12}$ (1722.03): C, 46.06; H, 1.99; N, 3.26. Found: C, 46.04; H, 1.98; N, 328. IR (KBr) ν_{max}: 1622 cm^{-1} (s,$\nu_{C=O}$), 1294 cm^{-1} (s), 1190 cm^{-1} (s), 1139 cm^{-1} (s, ν_{C-F}), 780 cm^{-1}(m, ν_{CF3}).

$Sm_2(BTP)_3(bpy)_2(CH_2Cl_2)_2$ (5). Yield: 93%. Elemental analysis (%) calcd for $C_{64}H_{38}Sm_2F_{18}N_4O_{12}Cl_4$ (1839.48): C, 41.79; H, 2.08; N, 3.05. Found: C, 41.76; H, 2.07; N, 3.03. IR (KBr) ν_{max}: 1616 cm^{-1} (s, $\nu_{C=O}$), 1294 cm^{-1} (s), 1190 cm^{-1} (s), 1139 cm^{-1} (s, ν_{C-F}), 780 cm^{-1} (m, ν_{CF3}).

$Sm_2(BTP)_3(phen)_2$ (6). Yield: 88%. Elemental analysis (%) calcd for $C_{66}H_{34}Sm_2F_{18}N_4O_{12}$ (1720.03): C, 46.15; H, 2.00; N, 3.26. Found: C, 46.17; H, 2.02; N, 3.28. IR (KBr) ν_{max}: 1622 cm^{-1} (s, $\nu_{C=O}$), 1294 cm^{-1} (s), 1187 cm^{-1} (s), 1137 cm^{-1} (s, ν_{C-F}), 778 cm^{-1}(m, ν_{CF3}).

Computational Details. The DFT-B3LYP (density functional method)[18] and CIS (configuration interaction with single excitations) approaches[19] using the 6-31G(d) basis set have been employed to optimize the geometry structures in the ground and excited states, respectively. On the basis of the optimized geometry structures in the ground and excited states, the absorption and emission properties in the acetonitrile media can be calculated by time-dependent density functional theory (TDDFT)[20] using 6-31G(d, p) basis set associated with the polarized continuum model (PCM).[21] All of the calculations

dx.doi.org/10.1021/ic302726z | Inorg. Chem. 2013, 52, 5013−5022

were accomplished by using the Gaussian 03 software package.[22] An analytical frequency analysis provides evidence that the calculated species represents a true minimum without imaginary frequencies on the respective potential energy surface. In the calculation of the optical absorption spectrum, the lowest spin-allowed singlet−singlet transitions, up to energy of ∼5 eV, were taken into account.

RESULTS AND DISCUSSION

Synthesis and Characterization of the Ligand and Complexes. The synthetic method of the complexes **1**−**6** is shown in Scheme 2. The IR spectra of both complexes **1** and **4** display the typical broad absorption in the region 3000−3500 cm^{-1}, corresponding to the presence of solvent molecules in the complexes **1** and **4**. In addition, the absence of the broad band in the region 3000−3500 cm^{-1} for complexes **2**, **3**, **5**, and **6** reveals that solvent molecules have been replaced by the bidentate neutral donors.[23] The carbonyl stretching frequency of BTP (1591 cm^{-1}) is red-shifted in complexes **1**−**6** (1619 cm^{-1} in **1**; 1618 cm^{-1} in **2**; 1623 cm^{-1} in **3**; 1621 cm^{-1} in **4**; 1616 cm^{-1} in **5**; 1622 cm^{-1} in **6**), which suggests the involvement of carbonyl oxygen in the complex coordinated with the Ln^{3+} ion. It is clear from the thermogravimetric analysis data that complex $Eu_2(BTP)_3(H_2O)_4$ undergoes a mass loss of about 5% (calcd 5.1%) in the first step (140−200 °C), which corresponds to the loss of the coordinated water molecules, and then, it undergoes a single step decomposition (Figure S3, Supporting Information). On the contrary, complexes **2** and **3** are more stable than complex $Eu_2(BTP)_3(H_2O)_4$, and they undergo single-step decomposition at 330 °C, illustrating that there are no solvents in complexes **2** and **3** (Figures S4 and S5, Supporting Information). Thermogravimetry differential scanning calorimetry (TG−DSC) curves of complexes $Sm_2(BTP)_3(H_2O)_4$ and **5** and **6** are similar to those of complexes $Eu_2(BTP)_3(H_2O)_4$ and **2** and **3** (Figures S6, S7, and S8, Supporting Information).

X-Ray Structural Characterization. X-ray crystallographic analysis reveals that complexes **1** and **4** and complexes **2** and **5** are isomorphic, respectively. Crystal data and data collection parameters for complexes **1**, **2**, **4**, and **5** are described in Table 1. The selected bond lengths and angles for complexes **1**,**2**, **4**, and **5** are described in Table S1 in the Supporting Information. The structural analysis reveals that complex **1**, crystallizing in the monoclinic space group *C*2/*c*, is a triple-stranded dinuclear helicate featured by the coordination of three bis-*β*-diketonate ligands to two crystallographically equivalent Eu^{3+} ions, as shown in Figure 1. The crystallographically distinct Eu^{3+} ion is ligated to six oxygen atoms from the three bis-diketonate and two oxygen atoms from DME, resulting in the distorted square antiprism geometry. The Eu−O distances are in the range of 2.339(4)−2.531(4) Å, which are in accordance with reported values in europium monodiketone complexes[24] and longer than reported values in europium bis-diketonate complexes.[14]

In the structure of complex **2** (Figure 2), two DME molecules are substituted by the ancillary ligand of bpy so that each central Eu^{3+} ion is coordinated with six oxygen atoms from three BTP ligands and two nitrogen atoms from bpy. The coordination geometry of the Eu^{3+} ion in complex **2** can be described as a distorted square antiprism. In complex **2**, the average bond distances of Eu−N and Eu−O are 2.587 Å and 2.341 Å, respectively; the asymmetric unit and coordination geometry of complexes **4** and **5** are given in Figures S9 and S10 in the Supporting Information. There is no classic hydrogen bond in the four complexes **1**, **2**, **4**, and **5**; interactions of C−H···F and C−H···O play a critical role in the stabilization of the structures. Nonclassic hydrogen bond lengths (Å) and angles (deg) for complexes **1**, **2**, **4**, and **5** are described in Table S2 in the Supporting Information.

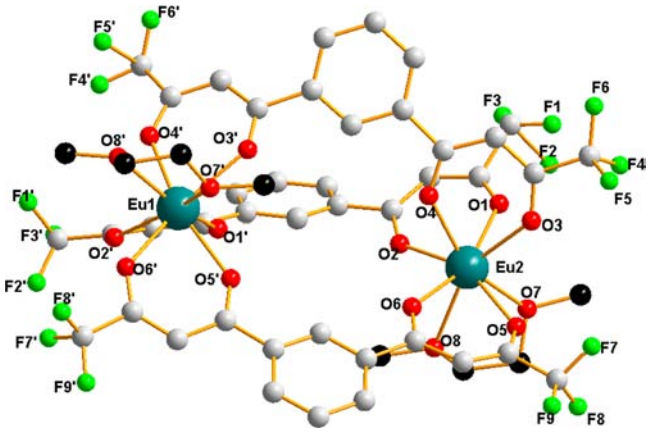

Figure 1. Molecular structure of complex **1**.

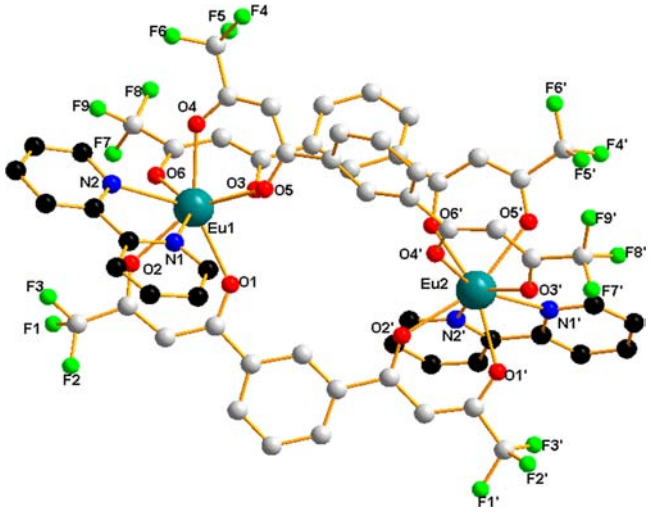

Figure 2. Molecular structure of complex **2**.

UV−Vis Spectra. The UV−vis absorption spectra of the free ligand BTP and complexes **1**−**3** were measured in CH_3CN solution ($c = 1 \times 10^{-5}$ M; Figure 3). The maximum absorption

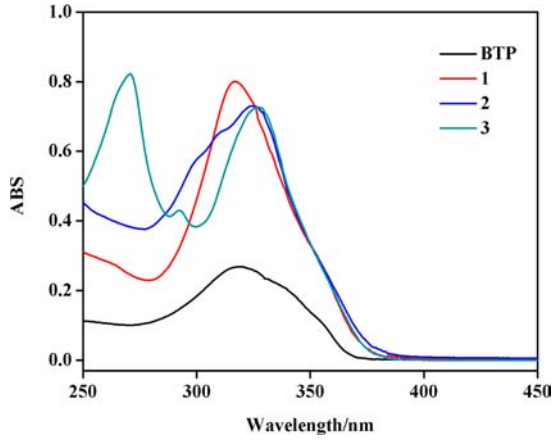

Figure 3. UV−vis absorption spectra of BTP, complexes **1**−**3** in CH_3CN ($c = 1 \times 10^{-5}$ M).

dx.doi.org/10.1021/ic302726z | Inorg. Chem. 2013, 52, 5013−5022

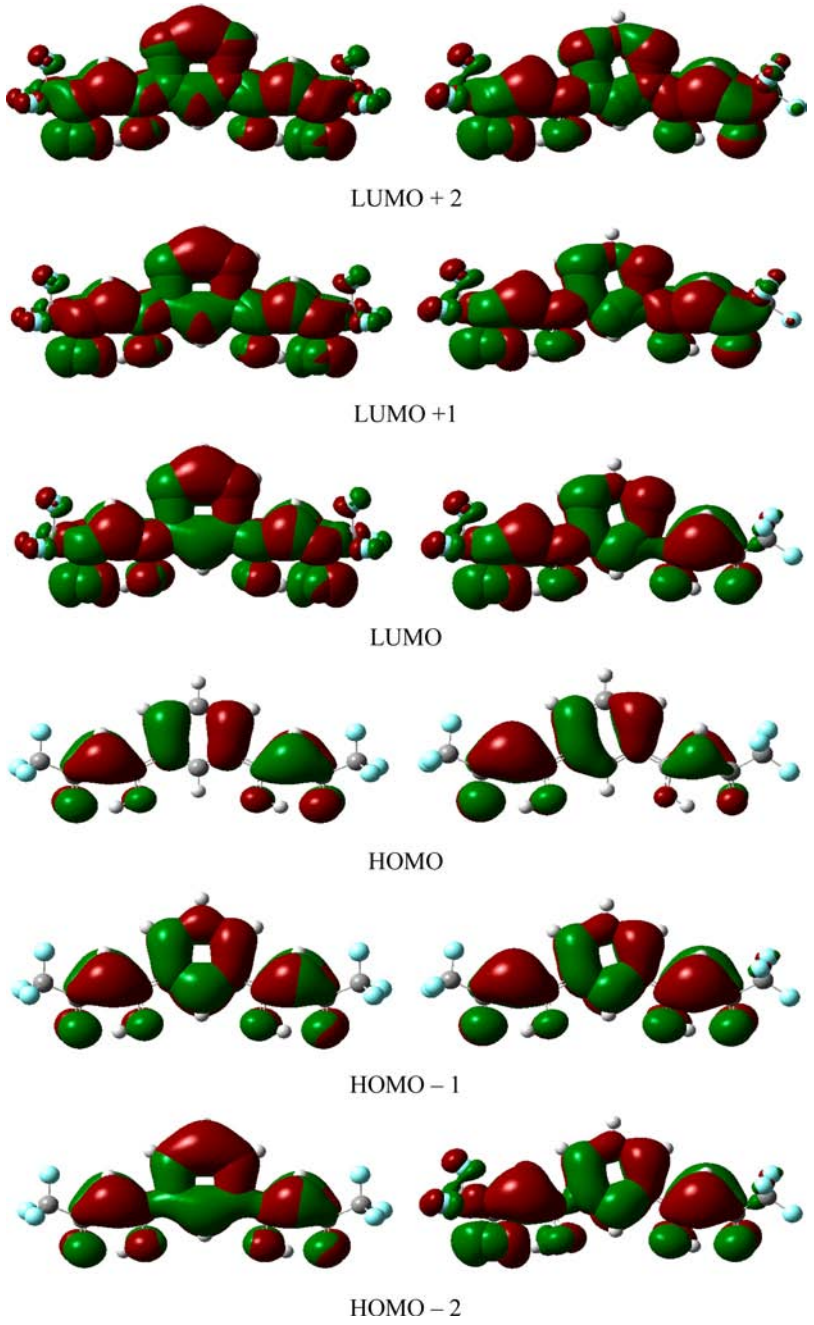

Figure 4. Spatial plots of the selected frontier molecular orbits of the ground (left) and excited (right) states of BTP.

band at 325 nm for BTP, is attributed to the singlet−singlet $\pi-\pi^*$ electronic transition of the aromatic rings in the bis-β-diketonate. Compared with the ligand, the maximum absorption peaks are blue-shifted or red-shifted for complexes **1**−**3**, which is attributed to the perturbation induced by the coordination of the Eu^{3+} ion. The spectral patterns of the Eu^{3+} complexes in CH_3CN are similar to that of the free ligand, indicating that the coordination of the europium ions does not significantly influence the energy of the singlet states of the bis-β-diketonate. The molar absorption coefficient values of complexes **1**−**3** are calculated as 8.00×10^4 (317 nm), 7.30×10^4 (325 nm), and 7.26×10^4 (327 nm) $mol^{-1}\cdot dm^3\cdot cm^{-1}$, respectively, which are about three times that of the ligand (2.68×10^4 $L\cdot mol^{-1}\cdot cm^{-1}$ at 325 nm), suggesting the presence of three ligands in the corresponding complexes.

Computational Studies. As shown in Figure 4, it is noted that the electronic cloud distribution of the HOMO in the ground and singlet excited state localizes at the COCHC(OH)PhC(OH)CHCO group, while the one of the LUMO localizes at the whole molecule. Herein, the HOMO and LUMO energies were calculated by DFT. The HOMO and LUMO levels for the ground and singlet excited state were found to be −6.69 and −2.59 eV and −6.42 and −2.61 eV, respectively. By comparison of the electronic cloud distribution of the HOMO in the ground, the electronic cloud distribution of the HOMO in the singlet excited state is asymmetrical, and one of two $-CF_3$ group have rotated to some extent. In addition to these above, the electronic cloud distribution of the $-CF_3$ group in the LUMO of the singlet excited state is poor,

dx.doi.org/10.1021/ic302726z | Inorg. Chem. 2013, 52, 5013−5022

Table 2. Absorptions of BTP Calculated with the TDDFT Methods

S_n	confign	CI codff	E/nm (eV)	oscillator	assignt
S_1	H→L	0.6409	328 (3.78)	0.0613	$JI_{COCHC(OH)C=C}$→JI^*_{BTP}
S_5	H−1→L	0.5325	313 (3.97)	1.1847	$JI_{COCHC(OH)PhC(OH)CHCO}$→$JI^*_{BTP}$
S_6	H−1→L+1	0.6238	289 (4.28)	0.0374	$JI_{COCHC(OH)PhC(OH)CHCO}$→$JI^*_{BTP}$

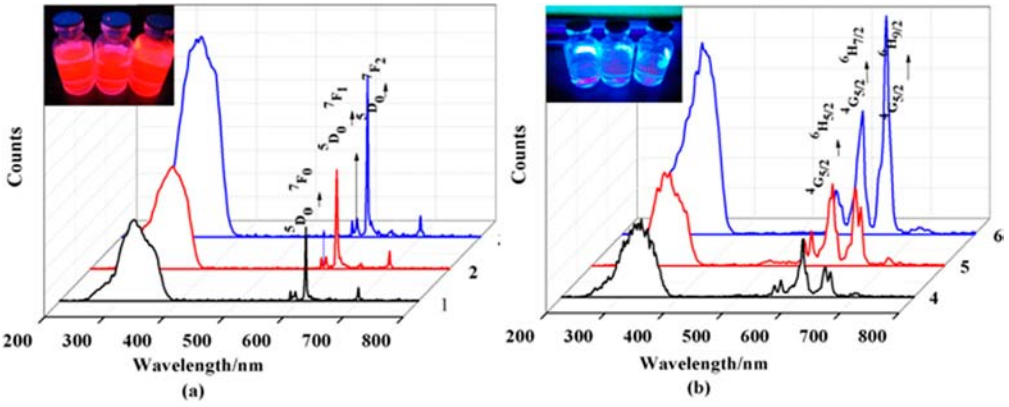

Figure 5. Excitation and emission spectra of complexes (a) **1**−**3** in CH_3CN (c = 1 × 10^{-5} M) and (b) **4**−**6** in CH_3CN (c = 1 × 10^{-5} M).

Table 3. Radiative (A_{RAD}) and Nonradiative (A_{NR}) Decay Rates, Observed Luminescence Lifetime (τ_{obs}), Intrinsic Quantum Yield (Φ_{ln}), Sensitization Efficiency (Φ_{sens}), and Overall Quantum Yield ($\Phi_{overall}$) for Complexes 1−3 and the Reported Analogous Lanthanide Complexes at 298 K

complexes	I_{7F2}/I_{7F1}	A_{RAD} (s^{-1})	A_{NR} (s^{-1})	τ_{obs} (us)	Φ_{ln} (%)	Φ_{sens} (%)	$\Phi_{overall}$ (%)
$Eu_2(BTP)_3(DME)_2$(1)	8.81	1032	6601	131	14	93	13
$Eu_2(BTB)_3(C_2H_5OH)_2(H_2O)_2$[14]	9.08	1207	2816	366	30	87	26
$Eu_2(BTP)_3(bpy)_2(CH_2Cl_2)_2)$(2)	12.43	1456	601	486	70	79	55
$Eu_2(BTB)_3(bpy)_2$[14]	18.30	1128	851	506	57	82	47
$Eu_2(BTP)_3(phen)_2$(3)	7.32	857	246	906	78	83	65
$Eu_2(BTB)_3(phen)_2$[14]	15.56	863	973	548	47	83	39

which matches well with the goal using the highly electron-withdrawing property of $-CF_3$ groups.

As shown in Table 2, the lowest excitation energy calculated by TD-DFT is 3.78 eV. It is obvious that S5 and S6 high-energy absorption transitions are mainly due to the HOMO − 1 → LUMO and HOMO − 1 → LUMO + 1 frontier molecular orbital transitions. The calculated singlet−singlet transitions of BTP are in reasonable agreement with the experimental data.

Photoluminescence (PL) Properties of Complexes 1−6. PL spectra of complexes **1**−**3** in CH_3CN are shown in Figure 5a.

In comparison with the absorption spectra of complexes **1**−**6**, the excitation spectra show narrow bands around 324 nm for **1**−**3** and 334 nm for **4**−**6**. Thus, the excitation and absorbance wavelength of complexes **1**−**6** overlap very well within the range, indicating characteristic lanthanide emission is sensitized through the ligand. Upon excitation at 324 nm, which is the maximum of the excitation spectrum, complexes **1**−**3** showed the characteristic emission bands of the Eu^{3+} ion corresponding to the $^5D_0 \rightarrow {}^7F_J$ (J = 0−4) transitions. Among them, the $^5D_0 \rightarrow {}^7F_2$ transition at λ = 612 nm is the strongest emission as an induced electric dipole transition, and its corresponding intensity is very sensitive to the coordination environment. This very intense $^5D_0 \rightarrow {}^7F_2$ peak, pointing to a highly polarizable chemical environment around the Eu^{3+} ion, is responsible for the brilliant red emission of complexes **1**−**3**.[25,26]

The intensity of the emission band at 592 nm is relatively weak and independent of the coordination environment because the corresponding transition $^5D_0 \rightarrow {}^7F_1$ is a magnetic transition. The intensity ratio of I_{7F2}/I_{7F1} is 8.81 for complex **1**, while it increased to 12.43 for **2** and 7.32 for **3**, suggesting that the Eu^{3+} ion is coordinated in a local site without any inversion center. Furthermore, the emission spectra of complexes **1**−**3** show only one peak for the $^5D_0 \rightarrow {}^7F_0$ transition and three stark components for the $^5D_0 \rightarrow {}^7F_1$ transition, indicating the presence of a single chemical environment around the Eu^{3+} ion. The emission bands around 582 and 650 nm are very weak, and owing to their corresponding transitions $^5D_0 \rightarrow {}^7F_{0,3}$ are forbidden both in magnetic and electric dipole schemes. The solid PL spectra of complexes **1**−**3** recorded at 298 K are shown in Figures S11−S13 in the Supporting Information. PL spectra of complexes **4**−**6** in CH_3CN are shown in Figure 4b. Upon excitation at 334 nm, which is the maximum of the excitation spectrum, complexes **4**−**6** show characteristic narrow band emissions of the Sm^{3+} ion corresponding to the $^4G_{5/2} \rightarrow {}^6H_J$ (J = 5/2, 7/2, 9/2, 11/2) transitions. The three expected peaks for the $^4G_{5/2} \rightarrow {}^6H_{5/2-9/2}$ transitions are well resolved. The most intense peak is the hypersensitive transition $^4G_{5/2} \rightarrow {}^6H_{9/2}$ at 650 nm.

The $^5D_0$ lifetimes (τ_{obs}) were determined from the luminescent decay profiles for complexes **1**−**3** at room temperature by fitting with monoexponential curves, proposing the presence of a single chemical environment around the emitting Eu^{3+} ion, and the values are compiled in Table 3. Typical decay profiles of complexes **1**−**3** are shown in Figure S14 in the Supporting Information. The relatively shorter

dx.doi.org/10.1021/ic302726z | Inorg. Chem. 2013, 52, 5013−5022

lifetime observed for complex **1** (τ_{obs} = 131 μs) can be caused by dominant nonradiative decay channels associated with vibronic coupling for the presence of water molecules, as well documented in many of the hydrated europium β-diketonate complexes. On the other hand, the relative longer lifetimes have been observed for complexes **2** (τ_{obs} = 486 μs) and **3** (τ_{obs} = 906 μs) because of their less important nonradiative deactivation pathways. The lifetimes observed for complexes **4** (τ_{obs} = 15 μs), **5** (τ_{obs} = 58 μs), and **6** (τ_{obs} = 100 μs) are relatively shorter than those of Eu^{3+} complexes. The decay profiles of complexes **4**–**6** are shown in Figure S15 in the Supporting Information.

The luminescence quantum yield Φ is an important parameter for evaluation of the efficiency of the emission process in luminescent materials. However, the overall quantum yield ($\Phi_{overall}$) of the lanthanide complex treats the system as a "black box" where the internal process is not explicitly considered. The overall luminescence quantum yield ($\Phi_{overall}$) for a lanthanide complex can be determined experimentally under excitation of the ligand. Given that the complex absorbs a photon, the sensitization efficiency can be defined as eq 2:[27]

$$\phi_{sens} = \frac{\phi_{overall}}{\phi_{ln}} \tag{2}$$

The intrinsic quantum yields of europium could not be determined experimentally upon direct f–f excitation because of very low absorption intensity. However, they can be estimated using eq 3, after calculating the radiative lifetime (τ_{rad}; eq 4):[28]

$$\phi_{ln} = \frac{A_{RAD}}{A_{RAD} + A_{NR}} = \frac{\tau_{obs}}{\tau_{rad}} \tag{3}$$

$$A_{RAD} = \frac{1}{\tau_{rad}} = A_{MD,0} n^3 \left(\frac{I_{tot}}{I_{MD}}\right) \tag{4}$$

where $A_{MD,0}$ = 14.65 s^{-1} is the spontaneous emission probability of the magnetic dipole $^5D_0 \rightarrow {}^7F_1$ transition, n is the refractive index of the medium, I_{tot} is the total integrated emission of the $^5D_0 \rightarrow {}^7F_J$ transitions, and I_{MD} is the integrated emission of the $^5D_0 \rightarrow {}^7F_1$ transition. A_{RAD} and A_{NR} are radiative and nonradiative decay rates, respectively.

The parameters characterizing the photophysical properties of solid-state samples of the complexes are summarized in Table 3. The overall luminescence quantum yield ($\Phi_{overall}$) observed for complex $Eu_2(BTP)_3(H_2O)_4$ is the lowest among the three complexes. It is understandable that the presence of the O–H oscillators in the close proximity of the Eu^{3+} center could effectively quench the luminescence *via* vibrational relaxations.[29] In addition, the substitution of four water molecules by two DME molecules in complex **1** results in an increase in emission intensity. On the other hand, the substitution of the solvent molecules by the bidentate nitrogen donors in complexes **2** and **3** lead to an increase in the observed quantum yields. Thus, complexes **1**–**3** show increasing luminescence quantum yields in a sequence of **1** < **2** < **3**, which is in agreement with the literature.[30,31] As such, a similar behavior is observed in determining the luminescence quantum yields of complexes **4**–**6** in acetonitrile solution (2% in **4**, 6% in **5**, 13% in **6**, respectively). In comparison with the luminescence quantum yields reported in the literature (Table 3), the overall quantum yields of complexes **2** and **3** separately rank the first among their analogues of complexes $Eu_2(BTB)_3L_2$ (BTB = 3,3′-bis(4,4,4-trifluoro-1,3-dioxobutyl)biphenyl, L = H_2O/C_2H_5OH, bpy, and phen). Perceptibly, the sensitization efficiency (Φ_{sens}) of BTP to the Eu^{3+} ion in complexes **1**–**3** is found to be promising.

To examine the effect of BTP on sensitizing Eu^{3+}luminescence, the luminescent signal intensities of complexes $Eu_2(BTP)_3(H_2O)_4$ and $Eu(BTFA)_3(H_2O)_2$ are compared in Figure 6. Although both ligands possess similar

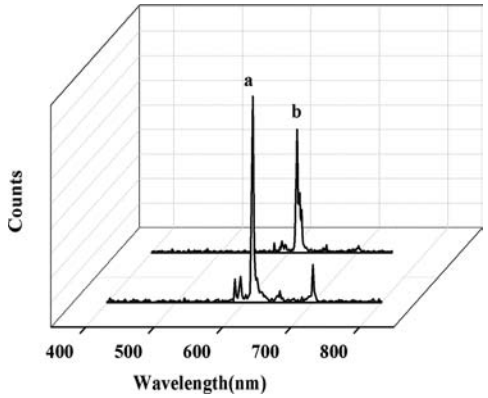

Figure 6. Emission spectra of isoabsorptive solutions (A = 0.1) of (a) $Eu_2(BTP)_3(H_2O)_4$ and (b) $Eu(BTFA)_3(H_2O)_2$ in CH_3CN, λ_{exc} = 350 nm.

triplet states, interestingly, the signal intensity of complex $Eu_2(BTP)_3(H_2O)_4$ is 1.67 times higher than that of the mononuclear analogue $Eu(BTFA)_3(H_2O)_2$. It proposes that BTP could be a better candidate on sensitizing Eu^{3+} ion luminescence than BTFA, which might be attributed to the rigidity of the triple-stranded helicate.[32] The rigid structure restricts the thermal vibration of the ligand and reduces the energy loss by radiationless decay.

Intramolecular Energy Transfer between Ligand and Eu^{3+} Ion. In general, the widely accepted energy transfer mechanism in lanthanide complexes is that proposed by Crosby et al.[31] In order to make energy transfer effective, the triplet states energy level of the ligand cannot be less than the $^5D_0$ level (17 500 cm^{-1}) of the Eu^{3+} ion. Moreover, the triplet states energy level of the ligand is close to the $^5D_1$ level (19 100 cm^{-1}), and the energy difference is about 1200 cm^{-1}, the strongest fluorescence emission that will occur. That is usually considered energy level matching.[33] To elucidate the energy transfer processes in the europium complex, the energy levels of the relevant electronic states should be estimated. The singlet and triplet energy levels of BTP and bidentate nitrogen donors are estimated by referring to their wavelengths of UV–vis absorbance edges and the lower wavelength emission peaks of the corresponding phosphorescence spectra. On account of the difficulty in observing the phosphorescence spectra of the ligand, the emission spectra of the complex $Gd_2(BTP)_3(H_2O)_4$ at 77 K can be used to estimate the triplet state energy level. Because the lowest lying excited level ($^6P_{7/2} \rightarrow {}^8S_{7/2}$) of Gd(III) is located at 32 150 cm^{-1}, the triplet state energy level of the ligand is not significantly affected by the Gd^{3+} ion.[34] As shown in Figure 5, the triplet energy level of $Gd_2(BTP)_3(H_2O)_4$, which corresponds to the lower emission peak wavelength, is 20 080 cm^{-1} (498 nm). The single state energy ($^1\pi\pi^*$) level of BTP is estimated by referencing its absorbance edge, which is 22 936 cm^{-1} (436 nm). The singlet levels of the ancillary

dx.doi.org/10.1021/ic302726z | Inorg. Chem. 2013, 52, 5013–5022

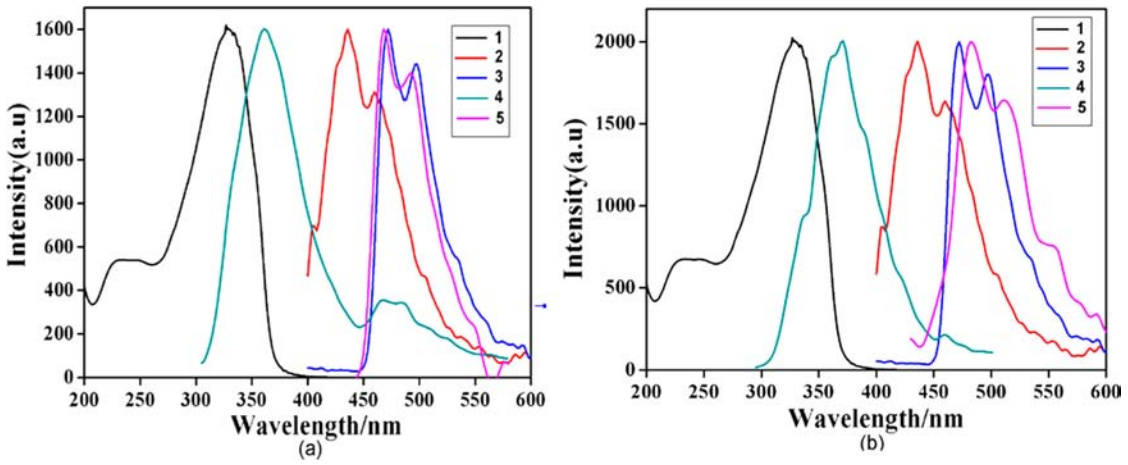

Figure 7. (a) (1) UV–vis absorption spectrum of BTP. (2) Room temperature emission spectrum of BTP. (3) Phosphorescence spectrum of $Gd_2(BTP)_3(H_2O)_4$ at 77 K. (4) Room temperature emission spectrum of bpy. (5) Phosphorescence spectrum of $Gd(bpy)_2(NO_3)_3$ at 77 K. (b) (1) UV–vis absorption spectrum of BTP. (2) Room temperature emission spectrum of BTP. (3) Phosphorescence spectrum of $Gd_2(BTP)_3(H_2O)_4$ at 77 K. (4) Room temperature emission spectrum of phen. (5) Phosphorescence spectrum of $Gd(phen)_2(NO_3)_3$ at 77 K.

ligands bpy (29 900 cm^{-1}) and phen (31 000 cm^{-1}) were taken from the literature.[35] The triplet (T1) energy levels of bpy and phen are calculated by referring to the lower wavelength emission edges of the corresponding phosphorescence spectra of Gd^{3+} complexes, which are 21 367 cm^{-1} (468 nm) and 20 790 cm^{-1} (481 nm), respectively (Figure 5a,b).

Generally, the sensitization pathway in luminescent europium complexes consists of excitation of the ligands into their excited singlet states, subsequent intersystem crossing of the ligands to their triplet states, and energy transfer from the triplet state to the ^5D_J manifold of the Eu^{3+} ion, followed by internal conversion to the emitting $^5D_0$ state; finally, the Eu^{3+} ion emits when transition to the ground state occurs. Moreover, the electron transition from the higher excited states, such as $^5D_3$ (24 800 cm^{-1}), $^5D_2$ (21 500 cm^{-1}), and $^5D_1$ (19 100 cm^{-1}), to $^5D_0$ (17 500 cm^{-1}) becomes feasible by internal conversion, and most of the photophysical processes take place in this orbital. Consequently, most europium complexes give rise to typical Eu(III) emission bands at ~581, 593, 614, 654, and 702 nm corresponding to the deactivation of the excited state $^5D_0$ to the ground states ^7F_J (J = 0–4). Therefore, the energy level's match of the triplet state of the ligands to $^5D_0$ of Eu^{3+} is one of the key factors which affect the luminescent properties of the properties of the europium complexes.[36]

To better investigate the energy transfer process between the ligand BTP and the neutral ligands, the overlap of the absorption and photoluminescence spectra of BTP and bidentate nitrogen donors should be discussed in detail. In a typical example of complex **2**, there is an overlap between the room temperature emission spectrum of bpy and the absorption spectra of the BTP in the region 307–372 nm (Figure 7a). It indicates that the radiative energy that comes from the singlet state of bpy can in part be absorbed by BTP. The singlet state of bpy can also transfer energy to the triplet level of BTP or to its own triplet level, which can be proved from the overlap between the room temperature emission of bpy and the phosphorescence spectra of $Gd_2(BTP)_3(H_2O)_4$ and $Gd(bpy)_2(NO_3)_3$. The singlet level of the BTP can transfer energy to the triplet state of bpy or to its own triplet level (overlap between the room temperature emission of BTP and the phosphorescence spectra of bpy or BTP). The triplet level of the neutral ligand, bpy, can also transfer energy to the central Eu^{3+} ion directly or through the triplet state of BTP (overlap of the phosphorescence spectra of $Gd_2(BTP)_3(H_2O)_4$ and $Gd(bpy)_2(NO_3)_3$). Similar processes can be observed for complex **3** (Figure 7b).

According to the above experimental results, the schematic energy level diagram and the energy transfer process that possibly takes place in complex **2** are shown in Figure 8. The

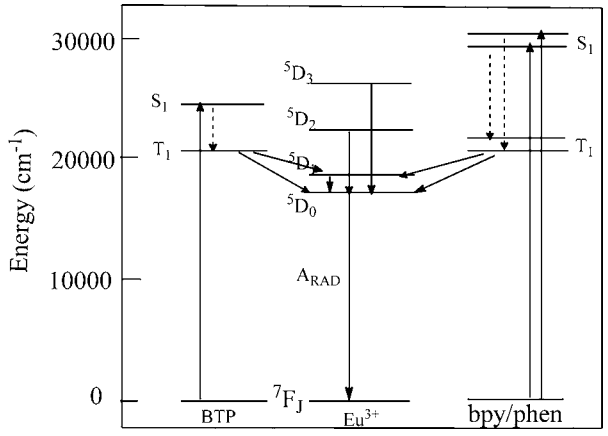

Figure 8. Schematic energy level diagram and energy transfer process for complex **2**. S1, first excited singlet state; T1, first excited triplet state.

triplet levels of the ligand BTP (20 080 cm^{-1}), bpy (21 367 cm^{-1}), and phen (20 709 cm^{-1}) are obviously higher than the $^5D_0$ level (17 500 cm^{-1}) of Eu^{3+} ion, and their energy gaps $\Delta E(^3\pi\pi^* - ^5D_0)$ are 2580, 3867, and 3209 cm^{-1}, respectively, which are too high to allow an effective back energy transfer. According to Latva's empirical rule,[33] an optimal ligand-to-metal energy transfer process for Eu^{3+} needs the energy gap $\Delta E(^3\pi\pi^* - ^5D_0) > 2500$ cm^{-1}; thus the ligand-to-metal transfer process could occur effectively for complexes **1**–**3**. At the same time, the $^4G_{5/2}$ level of the Sm^{3+} ion is 17 924 cm^{-1}, and the energy gaps $\Delta E(^3\pi\pi^* - ^4G_{5/2})$ are 2156, 3443, and 2785 cm^{-1}, respectively, which are too high to allow an effective back energy transfer. Moreover, the triplet levels of the ligand BTP (20 080 cm^{-1}) is also higher than the $^5D_1$ level (19 100 cm^{-1}) of the Eu^{3+} ion, thus energy transfer from the triplet state of

dx.doi.org/10.1021/ic302726z | Inorg. Chem. 2013, 52, 5013–5022

BTP to the $^5D_1$ level, followed by radiationless deactivation to the $^5D_0$ level. The energy gap between the $^1\pi\pi^*$ and $^3\pi\pi^*$ states of BTP, bpy, and phen are 2856, 8533, and 10 210 cm^{-1}, respectively. According to Reinhoudt's empirical rule, the intersystem crossing process becomes effective when ΔE ($^1\pi\pi^*-^3\pi\pi^*$) is at least 5000 cm^{-1}.[37] One can conclude that the effective intersystem crossing and ligand to metal energy transfer processes can be found in all complexes **1**–**3**, confirming that the ligands turn out to be quite efficient in sensitizing the Eu^{3+} ion luminescence.

CONCLUSIONS

The results of our work display a novel bis-β-diketonate ligand, which is a promising luminescence sensitizer on lanthanide ions, on the basis of the trifluorinated alkyl group. The characteristic emission spectra of Eu^{3+} complexes show a very high intensity for the hypersensitive $^5D_0 \rightarrow {}^7F_2$ transition, pointing to a highly polarizable chemical environment around the Eu^{3+} ion. Complex **1** displays efficient sensitized luminescence in acetonitrile solution (Φ_{sens} = 93%) with a quantum yield of 13%. Moreover, the displacement of the solvent molecules by bidentate nitrogen ligands enhances the metal-centered luminescence quantum yields, which were shown to exhibit exceptionally high PL quantum yields (55–65%) in complexes **2** and **3**. The results show that the substitution of solvent molecules by bidentate nitrogen ligands in $Eu_2(BTP)_3(DME)_2$ complex greatly enhances the metal-centered luminescence quantum yields and lifetime values. Notably, the signal intensity of bis-β-diketonate complex $Eu_2(BTP)_3(H_2O)_4$ is 1.67 times than that of complex $Eu(BTFA)_3(H_2O)_2$, although the ligands BTP and BTFA possess similar energy levels. The result might be attributed to rigidity of the triple-stranded helicate, which reduces the energy loss due to the vibration of the ligand. In conclusion, it opens up broad prospects for improving luminescent properties of Eu(III) complexes by the modification of β-diketonate ligands and therefore has potential applications in many photonic devices.

ASSOCIATED CONTENT

Supporting Information

Crystallographic data for complexes **1**, **2**, **4**, and **5**, NMR spectrum for BTP, ESI-TOF spectrum for BTP, TG-DSC curves for complexes $Eu_2(BTP)_3(H_2O)_4$, **2**, **3**, $Sm_2(BTP)_3(H_2O)_4$, **5**, and **6**, PL spectra of complexes **1**–**3** in the solid state, luminescence decay profiles of complexes **1**–**6**, and additional figures. This material is available free of charge via the Internet at http://pubs.acs.org.

AUTHOR INFORMATION

Corresponding Author

*E-mail: houyj@hlju.edu.cn; sunzz@hlju.edu.cn.

Notes

The authors declare no competing financial interest.

ACKNOWLEDGMENTS

We are grateful for financial support by National Natural Science Foundation of China (No. 50975058), Heilongjiang Province (Nos. B201207 and B201208), the Education Department of Heilongjiang Province of China (Nos.12511383 and 12521413), and Harbin Municipal Science and Technology Innovation Talents Special Funds Projects (No. RC2012XK001005).

REFERENCES

(1) Yu, J. B.; Zhou, L.; Zhang, H. J.; Zheng, Y. X.; Li, H. R.; Deng, R. P.; Peng, Z. P.; Li, Z. F. *Inorg. Chem.* **2005**, *44*, 1611–1618.

(2) (a) Zucchi, G.; Murugesan, V.; Tondelier, D.; Aldakov, D.; Jeon, T.; Yang, F.; Thuéry, P.; Ephritikhine, M.; Geffroy, B. *Inorg. Chem.* **2011**, *50*, 4851–4856. (b) Freund, C.; Porzio, W.; Giovanella, U.; Vignali, F.; Pasini, M.; Destri, S. *Inorg. Chem.* **2011**, *50*, 5417–5429. (c) Wang, H. H.; He, P.; Yan, H. G.; Gong, M. L. *Sens. Actuators B* **2011**, *156*, 6–11.

(3) (a) Piazza, E. D.; Norel, L.; Costuas, K.; Bourdolle, A.; Maury, O.; Rigaut, S. *J. Am. Chem. Soc.* **2011**, *133*, 6174–6176. (b) Bünzli, J.-C. G. *Chem. Rev.* **2010**, *110*, 2729–2755. (c) Shao, G. S.; Han, R. C.; Ma, Y.; Tang, M. X.; Xue, F. M.; Sha, Y. L.; Wang, Y. *Chem.—Eur. J.* **2010**, *16*, 8647–8651.

(4) (a) Shi, M.; Ding, C. R.; Dong, J. W.; Wang, H. Z.; Tian, Y. P.; Hu, Z. J. *Phys. Chem. Chem. Phys.* **2009**, *11*, 5119–5123. (b) Bünzli, J.-C. G.; Eliseeva, S. V. *Chem. Soc. Rev.* **2010**, *39*, 189–227.

(5) Jang, H.; Shin, C. H.; Jung, B. J.; Kim, D. H.; Shim, H. K.; Do, Y. *Eur. J. Inorg. Chem.* **2006**, 718–725.

(6) Wang, J. F.; Wang, R. Y.; Yang, J.; Zheng, Z. P.; Carducci, M. D.; Cayou, T. *J. Am. Chem. Soc.* **2001**, *123*, 6179–6180.

(7) (a) Melby, L. R.; Rose, N. J.; Abramson, E.; Caris, J. C. *J. Am. Chem. Soc.* **1964**, *86*, 5117. (b) Bauer, H.; Blanc, J.; Ross, D. L. *J. Am. Chem. Soc.* **1964**, *86*, 5125.

(8) (a) McGehee, M. D.; Bergstedt, T.; Zhang, C.; Saab, A. P.; O' Regan, M. B.; Bazan, G. C.; Srdanov, V. I.; Heeger, A. J. *Adv. Mater.* **1999**, *11*, 1349. (b) Yang, C. Y.; Srdanov, V.; Robinson, M. R.; Bazan, G. C.; Heeger, A. J. *Adv. Mater.* **2002**, *14*, 980.

(9) Sinha, S. P. *Complexes of the Rare Earth*; Pergamon: London, 1966.

(10) Binnemans, K. *Handbook on the Physics and Chemistry of Rare Earths*, Elsevier: Amsterdam, 2005; Vol. 35, pp 107–272.

(11) (a) Malta, O. L.; Brito, H. F.; Menezes, J. F. S.; Goncalvese Silva, F. R.; Donega, C. D.; Alves, S. *Chem. Phys. Lett.* **1998**, *282*, 233–238. (b) Xu, H.; Yin, K.; Huang, W. *J. Phys. Chem. C* **2010**, *114*, 1674–1683. (c) Ma, Y.; Wang, Y. *Coord. Chem. Rev.* **2010**, *254*, 972–990.

(12) (a) Grillo, V. A.; Seddon, E. J.; Grant, C. M.; Aromí, G.; Bollinger, J. C.; Folting, K.; Christou, G. *Chem. Commun.* **1997**, 1561–1562. (b) Aromí, G.; Berzal, P. C.; Gamez, P.; Roubeau, O.; Kooijman, H.; Spek, A. L.; Driessen, W. L.; Reedijk, J. *Angew. Chem., Int. Ed.* **2001**, *40*, 3444–3446. (c) Albrecht, M.; Schmid, S.; deGroot, M.; Weis, P.; Frohlich, R. *Chem. Commun.* **2003**, 2526–2527. (d) Clegg, J. K.; Lindoy, L. F.; McMurtriea, J. C.; Schilter, D. *Dalton Trans.* **2005**, 857–864.

(13) Bassett, A. P.; Magennis, S. W.; Glover, P. B.; Lewis, D. J.; Spencer, N.; Parsons, S.; Williams, R. M.; Cola, L. D.; Pikramenou, Z. *J. Am. Chem. Soc.* **2004**, *126*, 9413–9424.

(14) Li, H. F.; Yan, P. F.; Chen, P.; Wang, Y.; Xu, H.; Li, G. M. *Dalton Trans.* **2012**, *41*, 900–907.

(15) Zheng, Y. X.; Lin, J.; Liang, Y. J.; Lin, Q.; Yu, Y. N.; Meng, Q. G.; Zhou, Y. H.; Wang, S. B.; Wang, H. Y.; Zhang, H. J. *J. Mater. Chem.* **2001**, *11*, 2615–2619.

(16) He, P.; Wang, H. H.; Liu, S. G.; Shi, J. X.; Wang, G.; Gong, M. L. *Inorg. Chem.* **2009**, *48*, 11382–11387.

(17) (a) Shi, M.; Li, F. Y.; Yi, T.; Zhang, D. Q.; Hu, H. M.; Huang, C. H. *Inorg. Chem.* **2005**, *44*, 8929–8936. (b) Xu, H.; Wang, L. H.; Zhu, X. H.; Yin, K.; Zhong, G. Y.; Hou, X. Y.; Huang, W. *J. Phys. Chem. B* **2006**, *110*, 3023–3029.

(18) Runge, E.; Gross, E. K. U. *Phys. Rev. Lett.* **1984**, *52*, 997–1000.

(19) (a) Stanton, J. F.; Gauss, J.; Ishikawa, N.; Head Gordon, M. *J. Chem. Phys.* **1995**, *103*, 4160–4174. (b) Foreman, J. B.; Head-Gordon, M.; Pople, J. A. *J. Phys. Chem.* **1992**, *96*, 135–149. (c) Waiters, V. A.; Hadad, C. M.; Thiel, Y.; Colson, S. D.; Wiberg, K. B.; Johnson, P. M.; Foresman, J. B. *J. Am. Chem. Soc.* **1991**, *113*, 4782–4791.

(20) (a) Stratmann, R. E.; Scuseria, G. E.; Frisch, M. J. *J. Chem. Phys.* **1998**, *109*, 8218–8224. (b) Matsuzawa, N. N.; Ishitani, A. *J. Phys.*

Chem. A **2001**, *105*, 4953−4962. (c) Casida, M. E.; Jamorski, C.; Casida, K. C.; Salahub, D. R. *J. Chem. Phys.* **1998**, *108*, 4439−4449.
(21) (a) Cossi, M.; Scalmani, G.; Rega, N.; Barone, V. *J. Chem. Phys.* **2002**, *117*, 43−54. (b) Barone, V.; Cossi, M.; Tomasi, J. *J. Chem. Phys.* **1997**, *107*, 3210−3221.
(22) Frisch, M. J.; Trucks, G. W.; Schlegel, H. B.; Scuseria, G. E.; Robb, M. A.; Cheeseman, J. R.; Montgomery, J. A., Jr.; Vreven, T.; Kudin, K. N.; Burant, J. C.; Millam, J. M.; Iyengar, S. S.; Tomasi, J.; Barone, V.; Mennucci, B.; Cossi, M.; Scalmani, G.; Rega, N.; Petersson, G. A.; Nakatsuji, H.; Hada, M.; Ehara, M.; Toyota, K.; Fukuda, R.; Hasegawa, J.; Ishida, M.; Nakajima, T.; Honda, Y.; Kitao, O.; Nakai, H.; Klene, M.; Li, X.; Knox, J. E.; Hratchian, H. P.; Cross, J. B.; Bakken, V.; Adamo, C.; Jaramillo, J.; Gomperts, R.; Stratmann, R. E.; Yazyev, O.; Austin, A. J.; Cammi, R.; Pomelli, C.; Ochterski, J. W.; Ayala, P. Y.; Morokuma, K.; Voth, G. A.; Salvador, P.; Dannenberg, J. J.; Zakrzewski, V. G.; Dapprich, S.; Daniels, A. D.; Strain, M. C.; Farkas, O.; Malick, D. K.; Rabuck, A. D.; Raghavachari, K.; Foresman, J. B.; Ortiz, J. V.; Cui, Q.; Baboul, A. G.; Clifford, S.; Cioslowski, J.; Stefanov, B. B.; Liu, G.; Liashenko, A.; Piskorz, P.; Komaromi, I.; Martin, R. L.; Fox, D. J.; Keith, T.; Al-Laham, M. A.; Peng, C. Y.; Nanayakkara, A.; Challacombe, M.; Gill, P. M. W.; Johnson, B.; Chen, W.; Wong, M. W.; Gonzalez, C.; Pople, J. A. *Gaussian 03*, revision D.01; Gaussian, Inc.: Wallingford, CT, 2004.
(23) (a) De Silva, C. R.; Maeyer, J. R.; Wang, R. Y.; Nichol, G. S.; Zheng, Z. P. *Inorg. Chim. Acta* **2007**, *360*, 3543−3552. (b) Bellusci, A.; Barberio, G.; Crispini, A.; Ghedini, M.; Deda, M. L.; Pucci, D. *Inorg. Chem.* **2005**, *44*, 1818−1825.
(24) Van Meervelt, L.; Froyen, A.; D'Olieslager, W.; Walrand-Gorller, C.; Drisque, I.; King, G. S. D.; Maes, S.; Lenstra, A. T. H. *Bull. Soc. Chim. Belg.* **1996**, *105*, 377−381.
(25) Biju, S.; Ambili Raj, D. B.; Reddy, M. L. P.; Kariuki, B. M. *Inorg. Chem.* **2006**, *45*, 10651−10660.
(26) Werts, M. H. V.; Jukes, R. T. F.; Verhoeven, J. W. *Phys. Chem. Chem. Phys.* **2002**, *4*, 1542−154.
(27) Xiao, M.; Selvin, P. R. *J. Am. Chem. Soc.* **2001**, *123*, 7067−7073.
(28) (a) Chauvin, A. S.; Gumy, F.; Imbert, D.; Bunzli, J.-C. G. *Spectrosc. Lett.* **2004**, *37*, 517−532. (b) Chauvin, A. S.; Gumy, F.; Imbert, D.; Bunzli, J.-C. G. *Spectrosc. Lett.* **2007**, *40*, 193−193.
(29) (a) Peng, C. Y.; Zhang, H. J.; Yu, J. B.; Meng, Q. G.; Fu, L. S.; Li, H. R.; Sun, L. N.; Guo, X. M. *J. Phys. Chem. B.* **2005**, *109*, 15278−15287. (b) Wada, Y.; Okubo, T.; Ryo, M.; Nakazawa, T.; Hasegawa, Y.; Yanagida, S. *J. Am. Chem. Soc.* **2000**, *122*, 8583−8584.
(30) Fu, L.; Sá Ferreira, R. A.; Silva, N. J. O.; Fernandes, J. A.; Ribeiro-Claro, P.; Gonçalves, I. S.; de Zea Bermudez, V.; Carlos, L. D. *J. Mater. Chem.* **2005**, *15*, 3117−3125.
(31) Crosby, G. A.; Alire, R. M.; Whan, R. E. *J. Chem. Phys.* **1961**, *34*, 743−748.
(32) (a) Piguet, C.; Bernardinelli, G.; Hopfgartner, G. *Chem. Rev.* **1997**, *97*, 2005−2062. (b) Albrecht, M. *Chem. Rev.* **2001**, *101*, 3457−3497.
(33) Sato, S.; Wada, M. B. *Chem. Soc. Jpn.* **1970**, *43*, 1955.
(34) Wang, Y. W.; Zhang, Y. L.; Dou, W.; Zhang, A. J.; Qin, W. W.; Liu, W. S. *Dalton Trans.* **2010**, *39*, 9013−9021.
(35) Biju, S.; Ambili Raj, D. B.; Reddy, M. L. P.; Kariuki, B. M. *Inorg. Chem.* **2006**, *45*, 10651−10660.
(36) (a) Tanaka, M.; Yamagughi, G.; Shiokawa, J.; Yamanaka, C. B. *Chem. Soc. Jpn* **1970**, *43*, 549. (b) Haynes, A. V.; Drickamer, H. G. *J. Chem. Phys.* **1982**, *76*, 114.
(37) Steemers, F. J.; Verboom, W.; Reinhoudt, D. N.; Van der Tol, E. B.; Verhoeven, J. W. *J. Am. Chem. Soc.* **1995**, *117*, 9408−9414.